Int. J. Heat Mass Transfer. Vol. 32, No. 4, pp. 679–687, 1989
Printed in Great Britain

0017–9310/89 $3.00 + 0.00

Numerical simulation of Soret-induced double diffusion in an initially uniform concentration binary liquid

T. L. BERGMAN and R. SRINIVASAN
Department of Mechanical Engineering, University of Texas at Austin, Austin, TX 78712, U.S.A.

(*Received* 15 *March* 1988 *and in final form* 25 *August* 1988)

Abstract—The objective of this study is to determine the influence of Soret-induced solutal buoyancy forces on the hydrodynamics and heat transfer rates associated with the natural convection of an initially uniform concentration fluid contained in an enclosure with heated and cooled walls. Numerical predictions show that, for the case of opposing solutal and thermal buoyancy forces, Soret effects can induce thermal stagnation so that heat transfer across the enclosure is conduction dominated. Soret-induced buoyancy effects are, as expected, more pronounced at low thermal Rayleigh numbers. Contrary to expectations, however, augmenting solutal and thermal buoyancy forces also induce conduction dominated heat transfer across the enclosure, but the solutal buoyancy effects required to do so are very large. For real fluids, Soret contributions to the hydrodynamic mechanisms responsible for variations in heat transfer rates are apparently limited to water-based binary solutions operating near the density inversion temperature.

INTRODUCTION

RECENTLY, interest has developed concerning convective processes in fluid mixtures. In the case of binary liquids, double-diffusive effects [1] and coupled heat and mass transfer [2] can lead to an array of unexpected fluid motion and transport phenomena which is not well understood [3]. Since many industrially and environmentally relevant fluids are not pure, it has been suggested that more attention should be paid to convective phenomena which can occur in mixtures, but are not present in common fluids such as air or water [3].

Applications involving liquid mixtures include the casting of alloys, groundwater pollutant migration and separation operations. In all of these situations, multicomponent liquids can undergo natural convection driven by buoyancy forces resulting from simultaneous temperature and species gradients. In the case of binary mixtures, the species gradients can be established by the applied solutal boundary conditions, such as species rejection associated with alloy casting, or can be induced by coupled transport mechanisms, such as Soret (thermo) diffusion. In the case of Soret diffusion, species gradients are established in an otherwise uniform concentration mixture in accordance with the Onsager reciprocal relationships [2].

Extensive efforts have been made to focus exclusively on Soret phenomena and the resulting thermosolutal natural convection in initially uniform binary liquids. These efforts have been primarily concerned with the delay or triggering of convection in thin binary liquid layers heated from below or above and have been reviewed recently [3]. The details of these studies will not be repeated here. It is noted, however, that a main conclusion of the review is that Soret phenomena can never be ignored in binary liquids if the liquid undergoes natural convection. This conclusion is, at best, troubling when consideration is given to the standard engineering practice of ignoring the Soret and Dufour effects in multicomponent fluids [4, 5].

The reasons which are often cited for ignoring the Soret phenomenon are:

(a) the time scale associated with the establishment of Soret effects is large compared to the thermal time scale, due to the large Lewis numbers of binary liquids [6];

(b) compositional differences established by Soret effects will be washed out once convection begins [7];

(c) Soret diffusion coefficients for liquid mixtures are difficult to predict and experimental data are relatively scarce [2].

Each of these reasons should be carefully examined before ignoring Soret phenomena in the natural convection of liquid mixtures. For example, the first reason is not relevant to steady-state situations and may be irrelevant to convective flows in, for example, porous media characterized by interstitial pockets of liquid with small physical dimensions and, in turn, small Soret diffusion time scales. The second reason ought to be revised to consider the magnitude of the product of the diminished concentration difference and solutal expansion coefficient relative to thermal buoyancy forces, rather than the convectively diminished concentration differences alone. The final reason, although unfortunately true, cannot be used

NOMENCLATURE

A	aspect ratio, H/L
C	solute mass fraction
ΔC	dimensionless solute separation, $(C_{max}-C_{min})/C_i$
c_p	liquid specific heat
D	binary diffusion coefficient
g	gravitational acceleration
H	enclosure height
k	thermal conductivity
L	enclosure width
Le	Lewis number, α/D
$\overline{Nu}$	average Nusselt number
P	pressure
Pr	Prandtl number, ν/α
Ra	thermal Rayleigh number, $g\beta_t(T_2-T_1)L^3/\nu\cdot\alpha$
S	Soret number, $S_t(T_2-T_1)C_i(1-C_i)$
Sc	Schmidt number, ν/D
S_t	Soret diffusion coefficient
T	temperature
u, v	x- and y-velocity components
x	advection heat transfer parameter, $(\overline{Nu}-1)/(\overline{Nu}_0-1)$
x, y	horizontal and vertical Cartesian coordinates.

Greek symbols

α	thermal diffusivity, $k/\rho\cdot c_p$
β_c	solutal expansion coefficient, $\rho^{-1}\partial\rho/\partial C$
β_t	thermal expansion coefficient, $-\rho^{-1}\partial\rho/\partial T$
γ	stability parameter, $S_tC_i(1-C_i)\beta_c/\beta_t$
Γ	dimensionless solute concentration, $(C-C_{min})/(C_{max}-C_{min})$
θ	dimensionless temperature, $(T-T_2)/(T_1-T_2)$
μ	kinematic viscosity
ν	dynamic viscosity
ρ	mass density
ψ	dimensionless streamfunction.

Subscripts

i	initial
max	maximum
min	minimum
0	reference condition
1	left wall
2	right wall.

as a basis to neglect the potential influence of Soret phenomena in natural convection systems.

Due to apparent uncertainty regarding the relevance of Soret phenomena in the natural convection of binary liquids, a numerical investigation was conducted to determine under what conditions and to what magnitude Soret diffusion affects transport phenomena in these systems. Rather than considering the binary fluid layer heated from below or above, attention is directed toward a more conventional natural convection geometry: an enclosure with differentially heated side walls. This geometry is considered in this study because of applications and interest involving double-diffusive phenomena associated with lateral solidification of binary fluids.

NUMERICAL MODEL

The system under consideration is shown in Fig. 1 and consists of a two-dimensional enclosure of width L and height H which contains an initially uniform concentration binary liquid. The enclosure walls are maintained at prescribed temperatures while the top and bottom surfaces of the enclosure possess linear temperature distributions. Due to the imposed thermal boundary conditions, natural convection will occur in the liquid. The diffusing species separate by Soret effects which will, in turn, induce local solutal buoyancy forces in the fluid. In general, the buoyancy forces will either augment or counteract the thermal buoyancy forces in the system.

The governing equations which describe the system behavior are conservation of mass, momentum, energy and species. Coupling between the conserved quantities occurs due to thermal and solutal buoyancy contributions in the momentum equations and Soret diffusion of the solute. The thermophysical properties of the fluid are assumed to be constant, the Boussinesq approximation is invoked and the flow is treated as laminar, steady and two-dimensional. The Dufour effect is ignored since the species distribution is nearly uniform and viscous dissipation is neglected. With

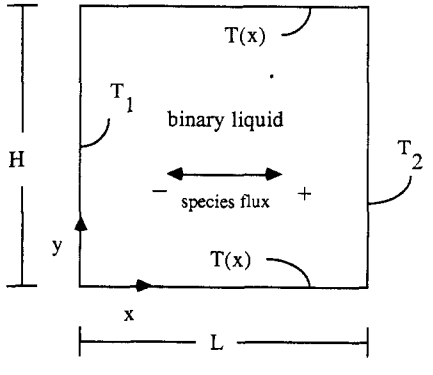

FIG. 1. Schematic of the physical system.

these approximations, the governing equations are

$$\frac{\partial}{\partial x}(\rho u)+\frac{\partial}{\partial y}(\rho v)=0 \tag{1}$$

$$\frac{\partial}{\partial x}(\rho uu)+\frac{\partial}{\partial y}(\rho uv)=\frac{\partial}{\partial x}\left(\mu\frac{\partial u}{\partial x}\right)+\frac{\partial}{\partial y}\left(\mu\frac{\partial u}{\partial y}\right)-\frac{\partial P}{\partial x} \tag{2}$$

$$\frac{\partial}{\partial x}(\rho uv)+\frac{\partial}{\partial y}(\rho vv)=\frac{\partial}{\partial x}\left(\mu\frac{\partial v}{\partial x}\right)+\frac{\partial}{\partial y}\left(\mu\frac{\partial v}{\partial y}\right)-\frac{\partial P}{\partial y}+g\beta_t\rho(T-T_0)-g\beta_0\rho(C-C_0) \tag{3}$$

$$\frac{\partial}{\partial x}(\rho uT)+\frac{\partial}{\partial y}(\rho vT)=\frac{\partial}{\partial x}\left(\frac{k}{c_p}\frac{\partial T}{\partial x}\right)+\frac{\partial}{\partial y}\left(\frac{k}{c_p}\frac{\partial T}{\partial y}\right) \tag{4}$$

$$\frac{\partial}{\partial x}(\rho uC)+\frac{\partial}{\partial y}(\rho vC)=\frac{\partial}{\partial x}\left(\rho D\frac{\partial C}{\partial x}\right)+\frac{\partial}{\partial y}\left(\rho D\frac{\partial C}{\partial y}\right)+\frac{\partial}{\partial x}\left(\rho DS_tC(1-C)\frac{\partial T}{\partial x}\right)+\frac{\partial}{\partial y}\left(\rho DS_tC(1-C)\frac{\partial T}{\partial y}\right) \tag{5}$$

where the last two terms on the right-hand side of equation (5) represent Soret diffusive effects [3].

The boundary conditions of the problem are associated with no slip, impermeable walls with specified constant temperatures (side walls) and linear temperature distributions (top and bottom)

$$u=v=0 \quad \text{at } x=0,L;\quad y=0,H \tag{6}$$

$$\frac{\partial C}{\partial x}=S_tC(1-C)\frac{\partial T}{\partial x} \quad \text{at } x=0,L \tag{7a}$$

$$\frac{\partial C}{\partial y}=S_tC(1-C)\frac{\partial T}{\partial y} \quad \text{at } y=0,H \tag{7b}$$

$$T=T_1 \quad \text{at } x=0 \tag{8a}$$

$$T=T_2 \quad \text{at } x=L \tag{8b}$$

$$T=T_1+(T_2-T_1)(x/L) \quad \text{at } y=0,H. \tag{8c}$$

The governing equations were discretized using the control volume approach of Patankar [8] while the power law formulation was employed to determine the combined advective and diffusive fluxes across the boundaries of each control volume. The discretized equations were solved iteratively with the line-by-line procedure of the tridiagonal matrix algorithm and the dynamic component of the pressure was calculated by the SIMPLER algorithm [8, 9]. The buoyancy forces in the y momentum equation (3) and the Soret diffusion effects in the species conservation equation (5) were treated as source terms. To enforce global species conservation, a residual concentration was determined at each iteration by spatially integrating and averaging the source terms of equation (5), subtracting the initial concentration C_i, and subsequently subtracting the residual from the newly predicted species concentration at each point in the computational domain. Upon convergence, the residual species concentration is zero and the average concentration is C_i.

A grid dependence study indicated that a 42×42 mesh was necessary to predict grid independent integral quantities, such as the total heat transfer rate across the cavity. Grid nodes were densely packed along the boundaries of the computational domain where steep solutal gradients and recirculations are initially predicted to occur. Specifically, the width and height of each control volume was increased relative to its neighboring control volume by 10% as the center of the computational domain was approached. Admittedly, the resolution of flow details in the center of the domain which become important only when solutal buoyancy forces are very large, may be compromised by the grid generation scheme.

In addition to the grid dependence study, the convective portion of the code was verified by comparing the predicted response of an air-filled enclosure to a benchmark numerical solution [10] while the numerical treatment of the diffusional Soret effects was validated by comparing the predicted one-dimensional species concentration distribution in a stagnant fluid with the exact solution [3]. The predicted heat transfer across the air-filled enclosure agreed to within 1% of the benchmark solution for $0<Ra<10^5$ while the predicted local species concentration variation from C_i, resulting from Soret effects, agreed to within 1% of the exact solution everywhere in the calculation domain.

RESULTS

Normalization of the governing equations yields the following dimensionless parameters which are relevant to the problem [3, 12]:

$$A=H/L \tag{9}$$

$$Ra=g\beta_t(T_2-T_1)L^3/(\nu\alpha) \tag{10}$$

$$Pr=\nu/\alpha \tag{11}$$

$$Sc=\nu/D \tag{12}$$

$$\gamma=S_tC_i(1-C_i)\beta_c/\beta_t \tag{13}$$

and

$$S=S_t\Delta TC_i(1-C_i). \tag{14}$$

The dimensionless parameters in equations (9)–(12) are the usual ones relevant in the natural convection of binary fluids. The stability parameter in equation (13), γ, is the ratio of the potential Soret-induced solutal buoyancy forces to thermally-induced buoyancy forces and can attain positive or negative values, depending on the sign of S_t. Although values of $|\gamma|$ are generally less than unity, $|\gamma|$ becomes infinite for

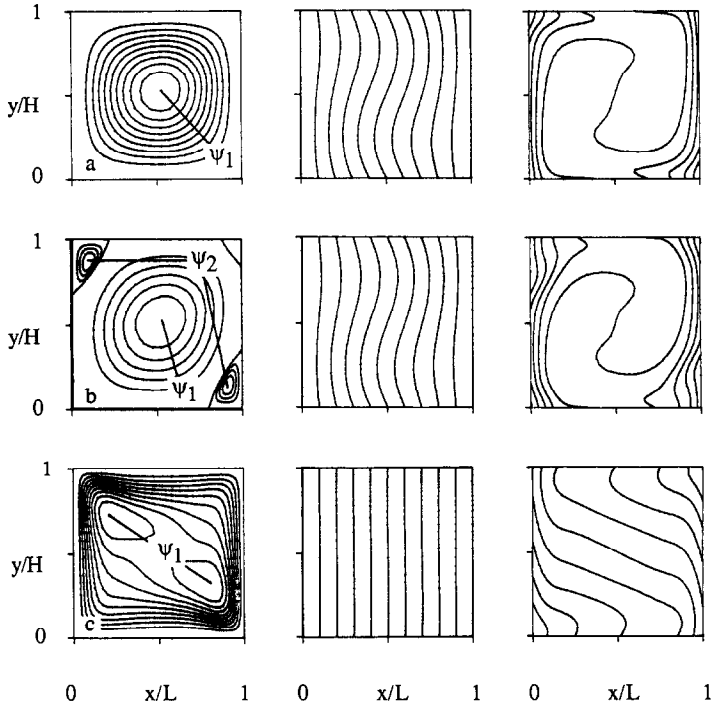

FIG. 2. Predicted streamlines (left), isotherms (middle) and concentration isopleths (right) for $A = 1$, $Ra = 10^3$, $Pr = 10$, $Le = 100$: (a) $\gamma = 0$, $\psi_1 = -123$; (*b*) $\gamma = -6$, $\psi_1 = -112$, $\psi_2 = 1.6$; (c) $\gamma = -7$, $\psi_1 = 4.6$.

water-based solutions at the density inversion temperature and can achieve values significantly greater than unity within 10°C of the inversion point [11], suggesting that solutal buoyancy forces due to Soret diffusion can dominate thermal buoyancy forces for certain binary fluids. The Soret number in equation (14), S, is an index of the potential species separation in the system but does not affect the system hydrodynamics. The ratio of the liquid thermal to species diffusivities is useful to consider and is represented by the Lewis number

$$Le = Sc/Pr = \alpha/D. \tag{15}$$

Representative results for the natural convection flow driven by combined thermal and Soret-induced solutal buoyancy forces are shown in Figs. 2–4 for various Ra and γ. In this study, reported results are for $A = 1$ and $S = 4.5 \times 10^{-5}$. To aid in the interpretation and discussion of the results, dimensionless streamfunctions, temperatures and concentrations are defined as follows.

The dimensionless streamfunction is evaluated from the pair of equations

$$\psi(x, y = 0) = \psi(x = 0, y = 0) - \frac{1}{\nu}\int_0^x v\,\mathrm{d}x \tag{16a}$$

and

$$\psi(x, y) = \psi(x, y = 0) + \frac{1}{\nu}\int_0^y u\,\mathrm{d}y \tag{16b}$$

where $\psi(x = 0, y = 0)$ is arbitrarily set to zero. The dimensionless temperature and species concentration are

$$\theta = (T - T_2)/(T_1 - T_2) \tag{17}$$

and

$$\Gamma = (C - C_{\min})/(C_{\max} - C_{\min}) \tag{18}$$

respectively.

Heat transfer rates across the cavity are described by the average Nusselt number

$$\overline{Nu} = \frac{1}{A(T_1 - T_2)}\int_{y=0}^{H} \left.\frac{\partial T}{\partial x}\right|_{x=0} \mathrm{d}y. \tag{19}$$

To orient the reader, thermal buoyancy forces induce clockwise rotation in all of the simulations while the Soret-induced buoyancy forces either oppose or augment their thermal counterparts. The initial concentration associated with the simulations is $C_i = 0.01$. The species separation associated with the simulations is $\Delta C = (C_{\max} - C_{\min})/C_i$ and, for $S = 4.5 \times 10^{-5}$, the maximum, ΔC (no convection), is 4.5×10^{-3}.

Predicted behavior associated with counteracting buoyancy forces

Figure 2 shows the predicted results for a system characterized by $Ra = 10^3$, $Pr = 10$ and $Le = 100$ for

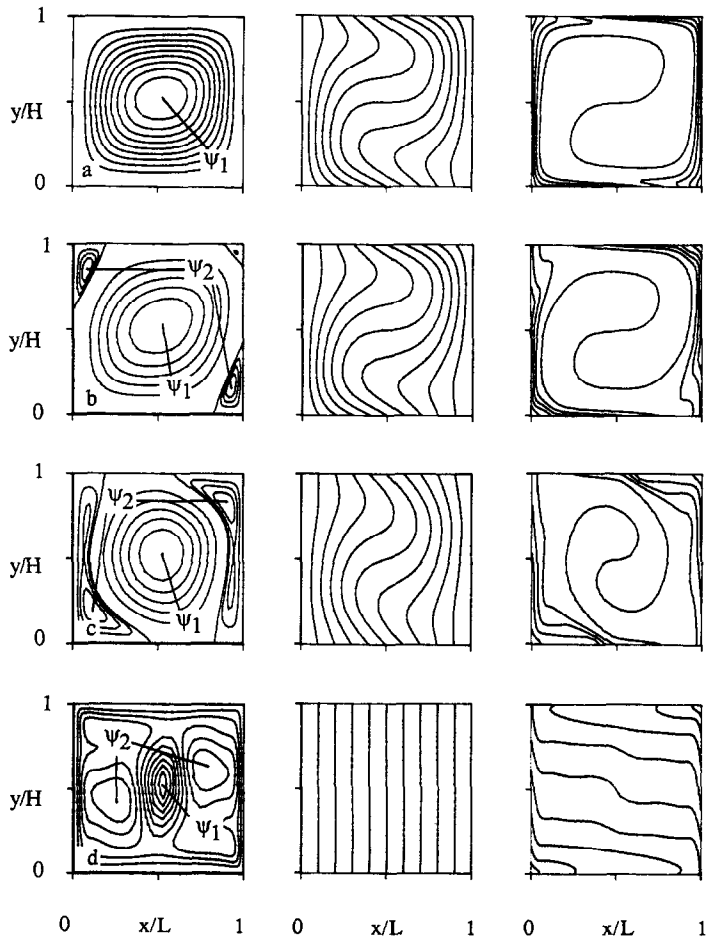

FIG. 3. Predicted streamlines (left), isotherms (middle) and concentration isopleths (right) for $A = 1$, $Ra = 10^4$, $Pr = 10$, $Le = 100$: (a) $\gamma = 0$, $\psi_1 = -649$; (b) $\gamma = -10$, $\psi_1 = -643$, $\psi_2 = 6.6$; (c) $\gamma = -16$, $\psi_1 = -283$, $\psi_2 = 21.4$; (d) $\gamma = -32$, $\psi_1 = -98.7$, $\psi_2 = 18.5$.

$\gamma = 0$ (Fig. 2(a)), $\gamma = -6$ (Fig. 2(b)), and $\gamma = -7$ (Fig. 2(c)).

The streamlines and isotherms of Fig. 2(a) ($\gamma = 0$) are the same as those in a pure fluid undergoing thermally-induced natural convection with clockwise flow existing throughout the system. The species distribution does not influence the system hydrodynamics and is determined by Soret-diffusive and advective transport mechanisms. The concentration isopleths, which are drawn at even Γ intervals between 0 and 1, are closely spaced near the heated and cooled side walls. In contrast, the concentration distribution is more uniform in the center of the computational domain where advective mixing is relatively strong.

Due to the rising and falling fluid on the hot and cold walls, respectively, and Soret diffusion of the heavy species toward warm temperatures, the maximum species concentration exists at the upper hot wall while the minimum species concentration is located at the bottom of the cold wall. The clockwise thermally-induced rotation pulls high concentration fluid from the upper hot wall to the upper cold wall and a similar phenomenon occurs for the low concentration fluid at the bottom of the system. The species separation is $\Delta C = 1.45 \times 10^{-4}$ (32% of the maximum diffusion value).

The results shown in Figs. 2(b) and (c) are for situations where the heavy species is diffused toward warm temperatures and solutal buoyancy forces are included in the analysis.

The results of Fig. 2(b), which are associated with $\gamma = -6$, show the anticipated solutally-driven recirculations in the upper left and lower right corners of the system. Also evident, however, are very weak recirculations in the opposing corners, driven by lateral solutal buoyancy forces. The center of the computation domain, which is characterized by a nearly uniform solute distribution, undergoes thermally-induced natural convection similar to that in Fig. 2(a). Due to mixing in the corners, the location of the maximum and minimum species concentrations have shifted to $y/H \approx 0.8$ and 0.2, respectively. The secondary recirculation increases ΔC relative to Fig. 2(a) to 1.57×10^{-4} as high and low concentration fluid is trapped in the corners.

As the counteracting solutal buoyancy forces are slightly increased ($\gamma = -7$, Fig. 2(c)), fundamentally different behavior is predicted to occur. The increased

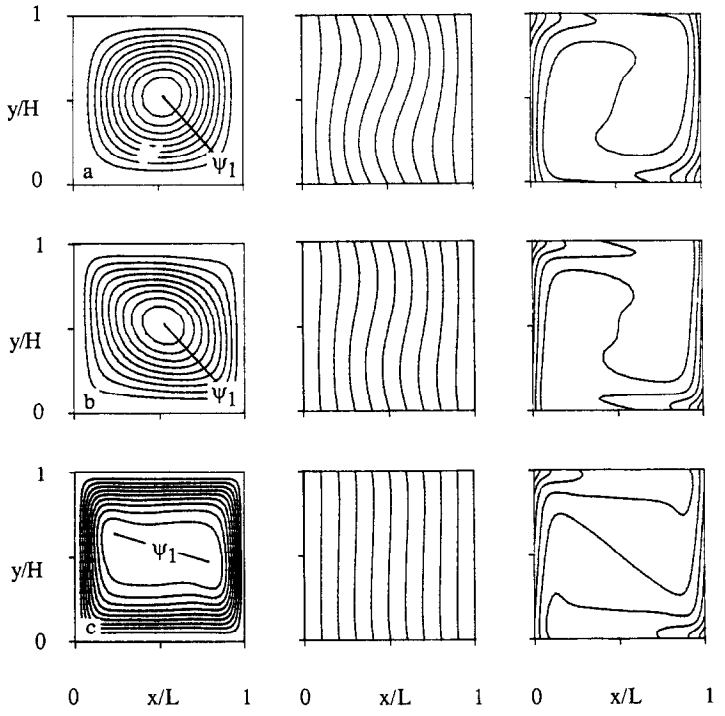

FIG. 4. Predicted streamlines (left), isotherms (middle) and concentration isopleths (right) for $A = 1$, $Ra = 10^3$, $Pr = 10$, $Le = 100$: (a) $\gamma = 0$, $\psi_1 = -123$; (b) $\gamma = 26$, $\psi_1 = -123$; (c) $\gamma = 30$, $\psi_1 = -17.5$.

solutal buoyancy forces induce global flow reversal, which is characterized by very small velocities, leading to thermal stagnation of the fluid layer. Due to the flow reversal, maximum and minimum species concentrations exist at the bottom of the warm wall and top of the cold wall, respectively. The fluid core is solutally stratified and the maximum species separation is $\Delta C = 2.52 \times 10^{-4}$.

As $|\gamma|$ is made larger than -7, the increased solutal buoyancy forces slightly increase the speed of the counterclockwise rotation in the system, but do not serve to increase $\overline{Nu}$ above unity. Hence, from a heat transfer perspective, counteracting solutal buoyancy forces decrease $\overline{Nu}$, as expected, and the results associated with Fig. 2 are $\overline{Nu} = 1.046$ for $\gamma = 0$, $\overline{Nu} = 1.023$ for $\gamma = -6$ and $\overline{Nu} = 1.000$ for $\gamma = -7$.

As previously discussed, compositional differences established by Soret effects are decreased as convective velocities are enhanced. Hence, the influence of γ, which is defined in terms of parameters which do not account for convective mixing, will vary as other Ra are considered. Specifically, smaller and larger $|\gamma|$ are necessary to influence the transport in the system as Ra is decreased and increased, respectively.

Figure 3 includes predicted results for $Ra = 10^4$, $Pr = 10$ and $Le = 100$ for $\gamma = 0$ (Fig. 3(a)), $\gamma = -10$ (Fig. 3(b)), $\gamma = -16$ (Fig. 3(c)), and $\gamma = -32$ (Fig. 3(d)).

The hydrodynamic and thermal results of Fig. 3(a) are similar to those of Fig. 2(a) except the fluid velocities are larger, resulting in increased heat transfer across the cavity. More significant variations exist in the species distributions of Figs. 2(a) and 3(a). In Fig. 3(a), the increased convective velocities decrease ΔC from 1.45×10^{-4} in Fig. 2(a) to 1.05×10^{-4}. In addition, the species boundary layers are thinner compared to those of Fig. 2(a) and solutally-stable species distributions develop along the right and left sides of the top and bottom enclosure surfaces, respectively, due to the significant vertical temperature gradients at these locations.

The results of Fig. 3(b), which are associated with $\gamma = -10$, show the same multicellular structure evident in Fig. 2(b). As expected, larger $|\gamma|$ is necessary to influence the hydrodynamic response of the system as Ra is increased. The species separation is $\Delta C = 1.30 \times 10^{-4}$.

While the convective flow for $Ra = 10^3$ was radically altered as γ was modestly increased from -6 to -7, results for $Ra = 10^4$ show that additional convective modes may occur. Figure 3(c) shows results for $\gamma = -16$. Here, the compressed concentration isopleths adjacent to the hot and cold vertical walls become sufficiently robust to induce downflow at the heated wall and upflow at the cooled wall while a thermally driven convection cell still exists in the center of the domain, where solutal gradients are very small. High and low concentration fluid is trapped in the side wall recirculations and $\Delta C = 1.45 \times 10^{-4}$.

As $|\gamma|$ is increased beyond a critical value ($\gamma = -32$, Fig. 3(d)) the convective flow is dominated by Soret-induced solutal buoyancy forces and the fluid layer becomes thermally stagnant. Further increases in $|\gamma|$ strengthen the degree of stagnation within the system.

Predicted heat transfer rates across the cavity decrease as solutal buoyancy forces resist thermally-

induced buoyancy forces in the liquid. Average Nusselt numbers for the results associated with $Ra = 10^4$ are 1.750, 1.639, 1.182 and 1.006 for Figs. 3(a)–(d), respectively.

Predicted behavior associated with augmenting buoyancy forces

The results so far show that Soret-induced buoyancy forces which oppose thermal buoyancy forces can, if sufficiently large, thermally stagnate the liquid within the enclosure. Heavy species can also be diffused to cold liquid regions so that solutal and thermal buoyancy forces, in a general sense, augment each other. As will become evident, however, augmenting buoyancy forces do not enhance convective heat transfer rates across the enclosure, as might be expected, but also serve to decrease heat transfer rates across the fluid layer.

Figure 4 shows typical results for augmenting buoyancy forces and includes those for a system characterized by $Ra = 10^3$, $Pr = 10$ and $Le = 100$ for $\gamma = 0$ (Fig. 4(a)), $\gamma = 26$ (Fig. 4(b)), and $\gamma = 30$ (Fig. 4(c)).

The streamlines, isotherms and concentration distributions of Fig. 4(a) are identical to those of Fig. 2(a) except the high concentration fluid is collected in the cool lower corner rather than the warm upper corner. The concentration separations in Figs. 4(a) and 2(a) are identical with $\Delta C = 1.45 \times 10^{-4}$.

The results of Fig. 4(b) ($\gamma = 26$) deviate from those associated with negative and zero γ. The structure of the main convective cell is changed and fluid which rises along the hot wall and falls at the cold wall penetrates further into the corners. This result is expected due to the inclusion of augmenting solutal buoyancy forces in the analysis. Due to increased vertical velocities (velocities near the side walls of the system have been increased by approximately 10% due to Soret effects), species advection across the enclosure is enhanced and evidence of the enhancement is noted near the top and bottom of the system where relatively low concentration fluid is carried from the top of the hot wall to the top of the cold wall and a similar phenomenon is evident at $y/H \approx 0$. As a consequence, although solute diffusional processes enhance the thermally-induced buoyancy forces at the vertical enclosure walls, the increased velocities resulting from this local augmentation serve to advect the solute in a manner which produces counteracting solutal buoyancy forces in the core of the fluid. The species separation in Fig. 4(b) is $\Delta C = 1.14 \times 10^{-4}$ and the overall Nusselt number has been decreased from $\overline{Nu} = 1.046$ in Fig. 4(a) to $\overline{Nu} = 1.020$.

As solutal buoyancy forces are increased further ($\gamma = 30$, Fig. 4(c)), the core of the enclosure becomes solutally stratified and discernible fluid motion is restricted to regions near the enclosure walls. As a result, the temperature distribution in the system is diffusion dominated and $\overline{Nu} = 1.002$ while $\Delta C = 1.23 \times 10^{-4}$.

Contrary to expectations, augmenting solutal buoyancy forces due to Soret diffusion decrease convective heat transfer rates across the enclosure for all of the simulations performed here. However, it is noted that large $|\gamma|$ are needed to affect convective heat transfer rates, relative to the results associated with negative γ, and few real fluids are characterized by positive γ of sufficient magnitude to reduce $\overline{Nu}$ significantly while retaining the validity of the Boussinesq approximation. For example, at $Ra = 10^4$, $Pr = 10$ and $Le = 100$, γ of order 100 is needed to stagnate the flow. The issue of fluids characterized by positive γ will not be addressed further and the interested reader is referred to ref. [12] where these effects are discussed in detail.

The influence of Soret-induced double diffusion on overall heat transfer rates

The representative results of Figs. 2–4 show that Soret-induced buoyancy forces can affect heat transfer rates across the enclosure which was considered in this study. The required solutal buoyancy forces necessary to impact $\overline{Nu}$ increase as Ra increases for the case of negative γ and large positive γ are required to modify $\overline{Nu}$.

The effect of γ on $\overline{Nu}$ for various Ra is summarized in Fig. 5 for $A = 1$ and $Pr = 10$. In this figure, a parameter representing the convective component of $\overline{Nu}$ is defined as

$$X = (\overline{Nu} - 1)/(\overline{Nu}_0 - 1) \tag{20}$$

where $\overline{Nu}_0$ corresponds to results for $\gamma = 0$. The results of Fig. 5 reflect the increasing influence of γ on $\overline{Nu}$ at smaller Ra, the existence of additional convective modes leading to partial reduction in X at higher Ra, and the greater influence of γ for cases where Soret-induced solutal buoyancy forces oppose thermal buoyancy forces in the system.

Since the results of Fig. 5 are limited to a certain fluid, geometry and applied thermal boundary conditions, additional simulations were performed for different boundary conditions (adiabatic top and

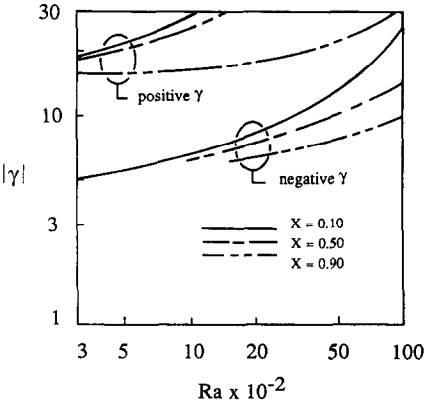

FIG. 5. The influence of γ on the convective component of the heat transfer across the enclosure, X, at various Ra for $A = 1$, $Pr = 10$, $Le = 100$.

bottom), enclosure aspect ratios and Pr. The results of these simulations indicate that the trends of Figs. 2–4 are independent of the thermal boundary conditions applied at $y = 0$ and H and the enclosure aspect ratio, for $0.5 < A < 2.0$. Results for liquid metals ($Pr = 0.01$, $Sc = 100$, $Le = 10^4$) show that the influence of γ on both the hydrodynamics and the heat transfer rates is negligible for $-1 < \gamma < 1$.

CONCLUSIONS

From the results, it is possible to conclude under what conditions Soret-induced buoyancy forces may (or may not) be important in the natural convection heat transfer of a binary liquid for the geometry considered here. Clearly, Soret diffusion effects usually do not need to be included in the analysis. However, situations exist where Soret effects should be accounted for. Since water-based binary liquids are usually characterized by $|\gamma|$ which exceeds unity only in the vicinity of the thermal inversion point, it may be necessary to include Soret phenomena in the analysis of freezing and melting of these liquids. Natural convection systems with applied thermal boundary conditions which bracket the density inversion temperature are susceptible to Soret phenomena if diffusing impurities exist in the liquid. Of course, the results for the Boussinesq fluid considered here may not be directly applicable to this situation. Finally, inclusion of Soret phenomena in the natural convection of liquid metals, which is known to be important in inducing thermal fluctuations in the near field adjacent to a solid/liquid interface during freezing [13] is apparently unnecessary if conditions in the far field are to be determined.

Acknowledgements—Support from the National Science Foundation under grant CBT-8552806 is gratefully acknowledged. The authors are grateful for computational facilities which were provided by the Department of Mechanical Engineering, University of Texas at Austin.

REFERENCES

1. H. E. Huppert and J. S. Turner, Double-diffusive convection, *J. Fluid Mech.* **106,** 299–329 (1981).
2. R. B. Bird, W. E. Stewart and E. N. Lightfoot, *Transport Phenomena.* Wiley, New York (1960).
3. J. K. Platten and J. C. Legros, *Convection in Liquids.* Springer, Berlin (1985).
4. E. R. G. Eckert and R. M. Drake, *Analysis of Heat and Mass Transfer.* McGraw-Hill, New York (1972).
5. W. M. Kays and M. E. Crawford, *Convective Heat and Mass Transfer.* McGraw-Hill, New York (1980).
6. C. F. Chen, Double-diffusive effects during solidification. In *Interdisciplinary Issues in Materials Processing and Manufacturing* (Edited by S. K. Samanta, R. Komanduri, R. McMeeking, M. M. Chen and A. Tseng, p. 527. ASME, New York (1987).
7. J. R. Carruthers, Dynamics of crystal growth. In *Crystal Growth: a Tutorial Approach* (Edited by W. Bardsley, D. T. J. Hurle and J. B. Mullin), p. 173. North-Holland, Amsterdam (1979).
8. S. V. Patankar, *Numerical Heat Transfer and Fluid Flow.* McGraw-Hill, New York (1980).
9. S. V. Patankar, A calculation procedure for two-dimensional elliptical situations, *Numer. Heat Transfer* **4,** 409–425 (1981).
10. G. de Vahl Davis, Natural convection of air in a square cavity: a bench mark numerical solution, *Int. J. Numer. Meth. Fluids* **3,** 249–264 (1983).
11. D. R. Caldwell, Soret coefficient of 1 N lithium iodide, *J. Phys. Chem.* **79,** 1882–1884 (1975).
12. R. Srinivasan, Numerical and experimental investigation of the influence of the Soret effect on natural convection in a binary liquid, M.S. Thesis, University of Texas at Austin, Austin, Texas (1988).
13. D. T. J. Hurle and E. Jakeman, Soret driven thermosolutal convection, *J. Fluid Mech.* **47,** 667–687 (1971).

SIMULATION NUMERIQUE DE LA DOUBLE DIFFUSION INDUITE DE SORET DANS UN LIQUIDE BINAIRE A CONCENTRATION INITIALE UNIFORME

Résumé—On détermine l'influence des forces de flottement solutales induite par effet Soret sur les flux hydrodynamiques et thermiques associés à la convection naturelle d'un fluide à concentration initiale uniforme, contenu dans une enceinte à parois chaudes et froides. Les prédictions numériques montrent que, pour le cas de forces de flottement thermique et solutal opposées, les effets Soret peuvent induire une stagnation thermique de telle façon que le flux thermique à travers la cavité est dominée par la conduction. Les effets de flottement sont, comme prévus, plus prononcés aux faibles nombres de Rayleigh thermique. Contrairement à ce qui est attendu, les forces croissantes de flottement thermique et solutal induisent aussi un transfert dominé par la conduction, mais les effets de flottement solutal doivent être très grands. Pour les fluides réels, les contributions Soret aux mécanismes hydrodynamiques responsables des variations des flux thermiques sont apparamment limitées aux solutions binaires aqueuses opérant près de la température d'inversion de densité.

NUMERISCHE SIMULATION DER SORET-INDUZIERTEN KONZENTRATIONSBEDINGTEN UND THERMISCHEN NATÜRLICHEN KONVEKTION IN EINER BINÄREN FLÜSSIGKEIT VON EINHEITLICHER ANFANGSKONZENTRATION

Zusammenfassung—Das Ziel dieser Untersuchung ist, den Einfluß der Soret-induzierten konzentrationsbedingten Auftriebskräfte auf die Strömungsmechanik und die Wärmeübertragung in Verbindung mit der natürlichen Konvektion einer Flüssigkeit zu bestimmen, welche anfangs eine gleichmäßige Konzentration aufweist und sich in einem Behälter mit geheizten und gekühlten Wänden befindet. Numerische Berechnungen für den Fall, daß die konzentrationsbedingten und die thermischen Auftriebseffekte einander entgegenwirken, zeigen, daß Soret-Effekte eine thermische Stagnation auslösen können, so daß die Wärmeübertragung durch den Behälter von der Wärmeleitung dominiert wird. Soret-induzierte Auftriebseffekte sind, wie erwartet, bei kleinen thermischen Rayleigh-Zahlen stärker ausgeprägt. Jedoch ergibt sich (entgegen der Erwartung) auch bei gleichsinniger Wirkung von konzentrationsbedingtem und thermischem Auftrieb eine von der Wärmleitung dominierte Wärmeübertragung im Behälter. Die erforderlichen Konzentrations-Auftriebskräfte sind jedoch sehr groß. Für reale Flüssigkeiten sind die Soret-Beiträge zum Strömungsmechanismus, der für die Schwankungen des Wärmeübertragungsvermögens verantwortlich ist, augenscheinlich auf die wäßrigen binären Lösungen beschränkt, die in der Nähe der Dichte-Umkehr-Temperatur arbeiten.

ЧИСЛЕННОЕ МОДЕЛИРОВАНИЕ ВЫЗВАННОЙ ЭФФЕКТАМИ СОРЭ ДИФФУЗИИ ТЕПЛА И МАССЫ В БИНАРНОЙ ЖИДКОСТИ С ПЕРВОНАЧАЛЬНО ОДНОРОДНОЙ КОНЦЕНТРАЦИЕЙ

Аннотация—Работа предпринята с целью определения влияния вызванных эффектами Сорэ подъемных сил в растворе на гидродинамику и интенсивность теплопереноса при естественной конвекции жидкости с первоначально однородной концентрацией, содержащейся в камере с нагреваемыми и охлаждаемыми стенками. Численные расчеты показывают, что в случае противоположно направленных концентационных и тепловых подъемных сил эффекты Сорэ могут привести к тепловому торможению, при котором теплоперенос поперек камеры определяется теплопроводностью. Вызванные эффектами Сорэ подъемные силы более существенны при низких значениях теплового числа Рэлея. Однако, вопреки ожиданиям, рост концентрационных и тепловых сил также приводит к преобладанию кондуктивного теплопереноса поперек камеры, но для этого требуются очень большие величины концентрационных подъемных сил. В случае реальных жидкостей влияние эффектов Сорэ на гидродинамические механизмы, обуславливающие изменение интенсивности теплопереноса, ограничиваются водными бинарными растворами при температуре, близкой к температуре инверсии плотности.